

# Armchair graphene nanoribbons in presence of line defect

Paramita Dutta,<sup>1,\*</sup> Santanu K. Maiti,<sup>2,†</sup> and S. N. Karmakar<sup>1,‡</sup>

<sup>1</sup>*Theoretical Condensed Matter Physics Division, Saha Institute of Nuclear Physics,  
Sector-I, Block-AF, Bidhannagar, Kolkata-700 064, India*

<sup>2</sup>*Physics and Applied Mathematics Unit, Indian Statistical Institute,  
203 Barrackpore Trunk Road, Kolkata-700 108, India*

The characteristics of energy band spectrum of armchair graphene nanoribbons in presence of line defect are analyzed within a simple non-interacting tight-binding framework. In metallic nanoribbons an energy gap may or may not appear in the band spectrum depending on the location of the defect line, while in semiconducting ribbons the gaps are customized, yielding the potential applicabilities of graphene nanoribbons in nanoscale electronic devices. With a more general model, we also investigate two-terminal electron transport using Green's function formalism.

PACS numbers: 73.22.Pr, 71.55.-i, 73.22.-f, 73.23.-b

## I. INTRODUCTION

The fabrication of single layer graphene by Novoselov *et al.*<sup>1</sup> in 2004 has opened a new era in the research of low-dimensional nanostructured materials. Graphene, the carbon allotrope with planar honeycomb lattice structure, is a promising candidate of nano-electronic components owing to its exceptional electronic, thermal and transport properties<sup>2</sup>. It has been predicted that graphene sheet is a zero gap semiconductor<sup>3</sup>, but its behavior strongly depends on the boundary conditions when it is tailored into ribbon, flake or tube<sup>4</sup>. The sensitivity to the ribbon width, chirality, shape of the edges has allowed one to switch its semiconductor-like behavior from zero gaped to the finite one. Intensive researches have already been done on graphene nanoribbons (GNRs) to explore the influence of edge topology<sup>5,6</sup> on transport properties. Some attempts including chemical doping<sup>7,8</sup>, application of uniaxial strain<sup>9,10</sup>, chemical edge modifications<sup>11</sup>, incorporation of impurity<sup>12</sup>, line defect<sup>13–17</sup> are in focus of study on this system. But to realize the potential application of this material the control over transport properties needs to be clarified in a deeper way.

To date, many theoretical<sup>18,19</sup> as well as experimental<sup>20,21</sup> works have been done which reveal the fact that graphene nanoribbons (GNRs) with zigzag edges exhibit a metallic phase with localized states located on the edges, while armchair graphene nanoribbons (AGNRs) show metallic or semiconducting phase depending on the width of the ribbons<sup>22–24</sup>. This phenomenon is true only for clean ribbons i.e., without any deformation anywhere in the sample. But, the presence of impurity or deformation makes the system behave differently. In 2007 Peeters *et al.*<sup>17</sup> have shown that in presence of line impurity in graphene nanoribbon a gap opens up in the energy band spectrum. The system they considered was practically coupled two graphene ribbons of different sizes separated by a distance. Line defect also yields the possibility of using graphene as a valley filter as demonstrated by Gunlycke *et al.*<sup>16</sup>. In a recent experiment topologi-

cal line defect has been studied using scanning tunneling microscope<sup>13,15</sup>. Although the studies involving AGNRs have already generated a wealth of literature there is still need to look deeper into the problem to address several important issues those have not been well explored ear-

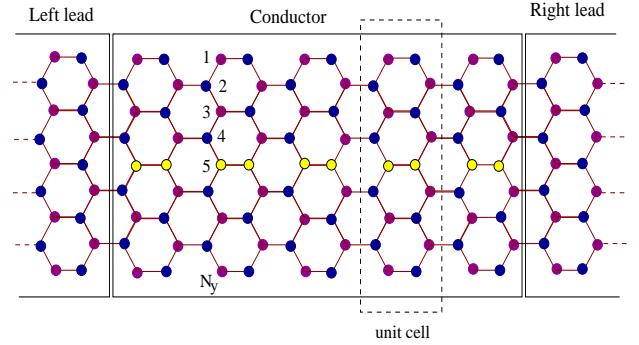


FIG. 1: (Color online). A schematic illustration of an armchair graphene nanoribbon, coupled to left and right leads, in presence of line defect (yellow circles). The blue and magenta circles represent two different sub-lattices of the ribbon.

lier, as for examples the understanding of the behavior of energy gap in metallic and semiconducting AGNRs in presence of line defect and also the dependence of this energy gap on the location of line defect. In the present work we mainly concentrate on these issues. Here we analyze the energy band structure of simple armchair graphene nanoribbons in presence of line defect within a tight-binding model. We show that depending on the location of a line defect in a metallic AGNR an energy gap may or may not appear in the band spectrum, while in a semiconducting AGNR the gap can be controlled. This phenomenon leads to the possibility of using AGNRs as nanoscale electronic devices. With a more specific model we also describe two-terminal electron transport using Green's function formalism to explore the results in realistic cases.

The structure of the paper is as follows. In Section II, we describe the specific model i.e., AGNR with side-attached leads and theoretical formulation to illus-

trate two-terminal electronic transport. The essential results are presented in Section III which contains (a) energy band structure of simple isolated armchair graphene nanoribbons in presence of line defect, and (b) transmission probability as a function of injecting electron energy through the lead-AGNR-lead bridge system. Finally, in Section IV, we summarize our main results and discuss their possible applications for further study.

## II. MODEL AND THEORETICAL FORMULATION

**Model:** Figure 1 presents a schematic illustration of the model quantum system, where a finite size AGNR is coupled to two semi-infinite graphene leads with arm-chair edges. The blue and magenta circles correspond to two different sublattices of the ribbon, and, the yellow circles, representing the defect sites, are arranged in a line result a defect line. A unit cell of the AGNR is described by the dashed region which contains  $2N_y$  atomic sites in our notation.

Our analysis for the present work is based on non-interacting electron picture, and, within this framework, tight-binding (TB) model is extremely suitable for analyzing electron transport through such a two-terminal bridge system. The single particle Hamiltonian which captures the AGNR and side-attached leads gets the form:

$$\mathbf{H} = \mathbf{H}_{\text{AGNR}} + \mathbf{H}_{\text{lead}} + \mathbf{H}_{\text{tun}}. \quad (1)$$

The first term  $\mathbf{H}_{\text{AGNR}}$  denotes the Hamiltonian of the AGNR sandwiched between two graphene leads. Under nearest-neighbor hopping approximation, the TB Hamiltonian of the AGNR reads,

$$\mathbf{H}_{\text{AGNR}} = \sum_l \epsilon_l c_l^\dagger c_l + \sum_l v_{l,l+1} (c_l^\dagger c_{l+1} + \text{h.c.}) \quad (2)$$

where,  $\epsilon_l$  is the on-site energy and  $v_{l,l+1}$  is the nearest-neighbor hopping integral. The hopping integral  $v_{l,l+1}$  is set equal to  $v$  or  $v'$  whether an electron hops between two ordered atomic sites or between two defect sites, and it is  $v''$  when the hopping of an electron takes place between an ordered and a defect site.  $c_l^\dagger$  ( $c_l$ ) is the creation (annihilation) operator of an electron at the site  $l$ .

The second and third terms of Eq. 1 correspond to the Hamiltonians for the semi-infinite graphene leads (left and right leads) and AGNR-to-lead coupling. A similar kind of TB Hamiltonian (see Eq. 2) is used to illustrate the leads where the Hamiltonian is parametrized by constant on-site potential  $\epsilon_0$  and nearest-neighbor hopping integral  $v_0$ . The AGNR is directly coupled to the leads by the parameters  $\tau_L$  and  $\tau_R$ , where they (coupling parameters) correspond to the coupling strengths between the edge sites of the ribbon and the left and right leads, respectively.

**Transmission probability:** To obtain electronic transmission probability through the AGNR we use Green's function formalism. Within the regime of coherent transport and in the absence of Coulomb interaction this technique is well applied. Using Fisher-Lee relation, two-terminal transmission probability  $T$  through the lead-AGNR-lead bridge system can be written as<sup>25</sup>,

$$T = \text{Tr} [\mathbf{\Gamma}_L \mathbf{G}_{\text{AGNR}}^r \mathbf{\Gamma}_R \mathbf{G}_{\text{AGNR}}^a] \quad (3)$$

where,  $\mathbf{\Gamma}_L$  and  $\mathbf{\Gamma}_R$  are the coupling matrices and  $\mathbf{G}_{\text{AGNR}}^r$  and  $\mathbf{G}_{\text{AGNR}}^a$  are the retarded and advanced Green's functions of the AGNR, respectively. Now the single particle Green's function operator representing the entire system for an electron with energy  $E$  is defined as,

$$\mathbf{G} = [(E + i\eta)\mathbf{I} - \mathbf{H}]^{-1} \quad (4)$$

where,  $\eta \rightarrow 0^+$ ,  $\mathbf{H}$  represents the Hamiltonian of the full system and  $\mathbf{I}$  is the identity matrix. Following the matrix forms of  $\mathbf{H}$  and  $\mathbf{G}$ , the problem of finding  $\mathbf{G}$  in the full Hilbert space of  $\mathbf{H}$  can be mapped exactly to a Green's function  $\mathbf{G}_{\text{AGNR}}$  corresponding to an effective Hamiltonian in the reduced Hilbert space of the AGNR itself and we get<sup>25</sup>,

$$\mathbf{G}_{\text{AGNR}} = [(E + i\eta)\mathbf{I} - \mathbf{H}_{\text{AGNR}} - \mathbf{\Sigma}_L - \mathbf{\Sigma}_R]^{-1}. \quad (5)$$

Here,  $\mathbf{\Sigma}_L$  and  $\mathbf{\Sigma}_R$  are the contact self-energies introduced to incorporate the effect of coupling of the AGNR to the left and right leads, respectively. Below we represent explicitly how these self-energies are evaluated for the graphene leads attached to the AGNR.

**Evaluation of self-energy:** In order to determine self-energies for these side-attached leads we follow the prescription addressed by Sancho *et al.*<sup>26</sup>, where both

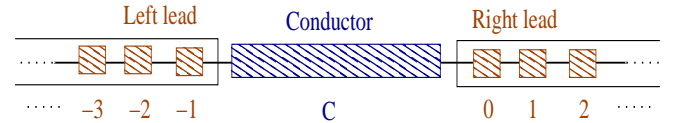


FIG. 2: (Color online). A schematic view of our model quantum system where AGNR and side-attached leads are sketched with discrete principal layers those are specified by integer numbers.

leads and AGNR are sketched with discrete effective principal layers. These layers are defined as the smallest group of neighboring atomic planes and they allow only nearest-neighbor interaction between them. It effectively transforms the original system into a linear chain of principal layers<sup>27</sup> as shown in Fig. 2. We label the principal layers in the right-lead as 0, 1, 2, ... and in the left-lead as -1, -2, -3, ... and so on. The sample between the leads is denoted by  $C$ . Below, we describe elaborately the evaluation of the self-energy corresponding to the right lead, and, following this prescription we also determine the self-energy for the left lead. Using Eq. 4 a set of

equations for the layer orbitals can be written as,

$$\begin{aligned}
[(E + i\eta)\mathbf{I} - \mathbf{H}_{0,0}]\mathbf{G}_{0,0} &= \mathbf{I} + \mathbf{H}_{0,1}\mathbf{G}_{1,0} \\
[(E + i\eta)\mathbf{I} - \mathbf{H}_{0,0}]\mathbf{G}_{1,0} &= \mathbf{H}_{0,1}^\dagger\mathbf{G}_{0,0} + \mathbf{H}_{0,1}\mathbf{G}_{2,0} \\
[(E + i\eta)\mathbf{I} - \mathbf{H}_{0,0}]\mathbf{G}_{2,0} &= \mathbf{H}_{0,1}^\dagger\mathbf{G}_{1,0} + \mathbf{H}_{0,1}\mathbf{G}_{3,0} \\
&\dots \\
[(E + i\eta)\mathbf{I} - \mathbf{H}_{0,0}]\mathbf{G}_{n,0} &= \mathbf{H}_{0,1}^\dagger\mathbf{G}_{n-1,0} + \mathbf{H}_{0,1}\mathbf{G}_{n+1,0}
\end{aligned} \tag{6}$$

where, we assume that  $\mathbf{H}_{0,0} = \mathbf{H}_{1,1} = \mathbf{H}_{2,2} = \dots$  and  $\mathbf{H}_{0,1} = \mathbf{H}_{1,2} = \mathbf{H}_{2,3} = \dots$ . Here,  $\mathbf{H}_{l,l}$  describes the Hamiltonian of  $l$ -th principal layer, while  $\mathbf{H}_{l,l+1}$  corresponds to the coupling matrix between  $l$ -th and  $(l+1)$ -th layers. The general expression of  $\mathbf{G}_{n,0}$  reads,

$$\mathbf{G}_{n,0} = t_0\mathbf{G}_{n-1,0} + \tilde{t}_0\mathbf{G}_{n+1,0} \tag{7}$$

where,

$$\begin{aligned}
t_0 &= [(E + i\eta)\mathbf{I} - \mathbf{H}_{0,0}]^{-1}\mathbf{H}_{0,1}^\dagger, \\
\tilde{t}_0 &= [(E + i\eta)\mathbf{I} - \mathbf{H}_{0,0}]^{-1}\mathbf{H}_{0,1}.
\end{aligned} \tag{8}$$

Substituting  $\mathbf{G}_{n,0}$  into the expressions of  $\mathbf{G}_{n-1,0}$  and  $\mathbf{G}_{n+1,0}$  we can write,

$$\mathbf{G}_{n,0} = t_1\mathbf{G}_{n-2,0} + \tilde{t}_1\mathbf{G}_{n+2,0} \quad (n \geq 2) \tag{9}$$

and this process continues iteratively to repeat. After  $i$ -th iteration we have,

$$\mathbf{G}_{n,0} = t_i\mathbf{G}_{n-2^i,0} + \tilde{t}_i\mathbf{G}_{n+2^i,0} \quad (n \geq 2^i) \tag{10}$$

with,

$$\begin{aligned}
t_i &= (\mathbf{I} - t_{i-1}\tilde{t}_{i-1} - \tilde{t}_{i-1}t_{i-1})^{-1}t_{i-1}^2, \\
\tilde{t}_i &= (\mathbf{I} - t_{i-1}\tilde{t}_{i-1} - \tilde{t}_{i-1}t_{i-1})^{-1}\tilde{t}_{i-1}^2.
\end{aligned} \tag{11}$$

The iteration is to be done until  $t_i, \tilde{t}_i \leq \delta$  with  $\delta$  arbitrarily small.

Using these  $t_i$ 's we can determine the Green's function of a single layer in terms of the Green's function of the following or preceding one like,

$$\mathbf{G}_{1,0} = \mathbf{T}\mathbf{G}_{0,0} \quad \text{and} \quad \mathbf{G}_{0,0} = \tilde{\mathbf{T}}\mathbf{G}_{1,0} \tag{12}$$

where,  $\mathbf{T}$  is the transfer matrix and it is defined as,

$$\begin{aligned}
\mathbf{T} &= (t_0 + \tilde{t}_0t_1 + \tilde{t}_0\tilde{t}_1t_2 + \dots + \tilde{t}_0\tilde{t}_1\tilde{t}_2\dots t_n), \\
\tilde{\mathbf{T}} &= (\tilde{t}_0 + t_0\tilde{t}_1 + t_0t_1\tilde{t}_2 + \dots + t_0t_1\tilde{t}_2\dots \tilde{t}_n).
\end{aligned} \tag{13}$$

After some algebraic calculations we can write from Eq. 6,

$$\mathbf{G}_{0,0} = [(E + i\eta)\mathbf{I} - \mathbf{H}_{0,0} - \mathbf{H}_{0,1}\mathbf{T}]^{-1}. \tag{14}$$

With this formalism, the surface Green's function of the left and right leads can be found as,

$$\begin{aligned}
\mathbf{g}_{-1,-1}^L &= [(E + i\eta)\mathbf{I} - \mathbf{H}_{0,0} - \mathbf{H}_{-2,-1}^\dagger\tilde{\mathbf{T}}]^{-1} \\
\mathbf{g}_{0,0}^R &= [(E + i\eta)\mathbf{I} - \mathbf{H}_{0,0} - \mathbf{H}_{0,1}\mathbf{T}]^{-1}
\end{aligned} \tag{15}$$

where,  $\mathbf{H}_{0,0}$  and  $\mathbf{H}_{-2,-1}$  are the Hamiltonians for a principal layer in both layer and the tunneling matrix between two principal layers in the right-lead, respectively. The main advantage of this framework<sup>28-30</sup> rather than any other method is that here the number of iterations required for convergence is very small<sup>31,32</sup>. Finally, we get the expressions for the self-energies of the two leads as,

$$\begin{aligned}
\Sigma_L &= \mathbf{H}_{-1,C}^\dagger \mathbf{g}_{-1,-1}^L \mathbf{H}_{-1,C}, \\
\Sigma_R &= \mathbf{H}_{C,0} \mathbf{g}_{0,0}^R \mathbf{H}_{C,0}^\dagger
\end{aligned} \tag{16}$$

where,  $\mathbf{H}_{0,1}$  and  $\mathbf{H}_{1,2}$  are left lead-to-AGNR and AGNR-to-right lead coupling matrices, respectively. Using the above expressions of self-energies for the graphene leads we evaluate effective Green's function  $\mathbf{H}_{\text{AGNR}}$  with the help of Eq. 5 and then calculate two-terminal transmission probability.

### III. RESULTS AND DISCUSSION

In this section we present analytical results of energy band spectrum for isolated AGNRs and numerical results computed for transmission probability through AGNRs under conventional biased conditions. Throughout our analysis we set the on-site energies in the two side-attached graphene leads to zero,  $\epsilon_0 = 0$ , and in the AGNR  $\epsilon_l = 0$  for ordered sites, while  $\epsilon_l = 1\text{eV}$  for defect sites. The nearest-neighbor coupling strength in the leads ( $v_0$ ) is fixed at 1eV, and the coupling parameters  $\tau_L$  and  $\tau_R$  are also set at 1eV. In AGNR, sandwiched between two leads, we use three different hopping integrals,  $v, v'$  and  $v''$ , and their values are fixed at 1eV, 0.7eV and 0.1eV, respectively. We fix the equilibrium Fermi energy  $E_F$  at zero and choose the units where  $c = e = h = 1$ . The energy scale is measured in unit of  $v$ .

#### A. AGNR without side-attached leads: Energy band structure and related issues

To find the energy dispersion relation of a finite width AGNR we establish an effective difference equation analogous to the case of an infinite one-dimensional chain. This can be done by proper choice of a unit cell (see Fig. 1) from the nano-ribbon. With this configuration, the effective difference equation of the AGNR reads,

$$(\mathcal{E}\mathbf{I} - \mathcal{E})\psi_j = \mathcal{T}\psi_{j+1} + \mathcal{T}^\dagger\psi_{j-1} \tag{17}$$

where,

$$\psi_j = \begin{pmatrix} \psi_{j1} \\ \psi_{j2} \\ \psi_{j3} \\ \vdots \\ \psi_{j2N_y} \end{pmatrix}. \tag{18}$$

In the above relation,  $\mathcal{E}$  and  $\mathcal{T}$  correspond to the site-energy and nearest-neighbor hopping matrices of the unit cell, respectively, and  $\mathcal{I}$  is the identity matrix. The dimension of these three matrices is  $(2N_y \times 2N_y)$ . Since in the nano-ribbon translational invariance exists along the

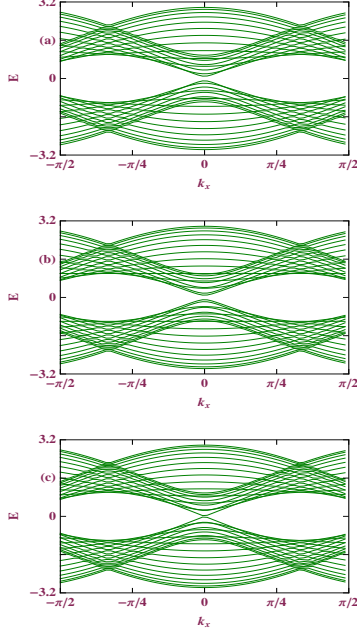


FIG. 3: (Color online). Energy band diagrams of armchair graphene nanoribbons in absence of any line defect, where (a)  $N_y = 18$ , (b)  $N_y = 19$ , and (c)  $N_y = 20$ .

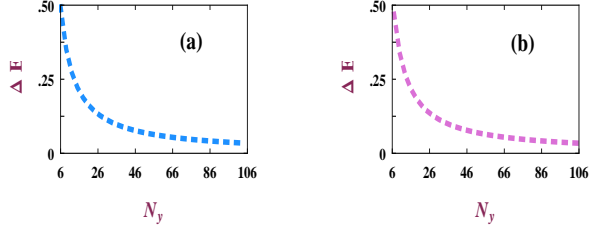


FIG. 4: (Color online). Energy gap  $\Delta E$ , at  $k_x = 0$ , as a function of ribbon width  $N_y$ . (a)  $N_y = 3n$  and (b)  $N_y = 3n + 1$ , where  $n$  is an integer.

$x$ -direction, we can write  $\psi_j$  in terms of the Bloch waves and then Eq. 17 gets the form,

$$(E\mathcal{I} - \mathcal{E}) = \mathcal{T}e^{ik_x\Lambda} + \mathcal{T}^\dagger e^{-ik_x\Lambda} \quad (19)$$

where,  $\Lambda = 3a$  is the spacing between two neighboring unit cells.  $a$  is the length of each side of hexagonal benzene like ring. Solving Eq. 19 we find the desired energy dispersion relation ( $E$  vs.  $k_x$ ) of the armchair ribbon.

As illustrative examples, in Fig. 3 we present the energy band diagrams of AGNRs for three different ribbon widths when they are free from any line defect. In this

spectra the three typical numbers (18, 19 and 20) of  $N_y$  are chosen only to make  $N_y$  in the forms  $3n$ ,  $3n + 1$  and  $3n + 2$ , respectively, since the energy band structures of AGNRs are highly sensitive to these typical ribbon widths<sup>22</sup>. Here we set  $n = 6$ . From the spectra it is observed that for the particular case where  $N_y = 3n + 2$ , the lowest conduction band and the highest valence band coincides with each other at  $k_x = 0$ , resulting zero energy gap in the band spectrum (Fig. 3(c)). This indicates metallic phase of the AGNR. However, for the other two cases ( $N_y = 3n$  and  $3n + 1$ ), a finite gap in the band spectrum is obtained at  $k_x = 0$  representing the semiconducting behavior. In these three spectra (Figs. 3(a)-(c)) since

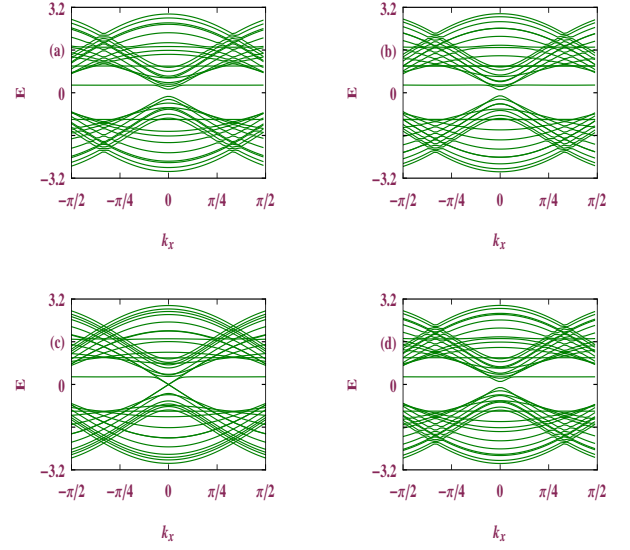


FIG. 5: (Color online). Energy band diagrams of armchair graphene nanoribbons in presence of line defect. (a)  $N_y = 18$ ,  $N_i = 5$ ; (b)  $N_y = 19$ ,  $N_i = 4$ ; (c)  $N_y = 20$ ,  $N_i = 6$  and (d)  $N_y = 20$ ,  $N_i = 5$ .  $N_i$  describes the location of a defect line.

$N_y$  is finite, the wavevector along  $y$ -direction becomes quantized and for each value of  $k_y$  we get a  $E$ - $k_x$  curve which results distinct energy levels in the  $E$ - $k_x$  diagram. For large enough  $N_y$ , energy gaps between these energy levels decrease sharply, and therefore, quasi-continuous energy bands are formed. The energy gaps between the conduction and valence bands, at  $k_x = 0$ , of AGNRs with  $N_y = 3n$  and  $N_y = 3n + 1$  strongly depend on the value of  $n$  i.e., ribbon width. To reveal this fact in Fig. 4 we present the variation of energy gap  $\Delta E$  as a function of  $N_y$  for two different cases. It shows that the energy gap sharply decreases with  $N_y$  when  $N_y$  becomes smaller, but it eventually saturates to a finite non-zero value, though it is too small, for large enough  $N_y$ . So, in short, we can emphasize that a metallic phase is observed for AGNRs when  $N_y = 3n + 2$ , while the semiconducting phase is visible for the AGNRs with  $N_y = 3n$  and  $3n + 1$ .

The results described above for clean nanoribbons i.e., nanoribbons in absence of any line defect have already been established in the literature, but the central issue



of our present investigation - the interplay between the existence of a line defect, the width of AGNRs and the location of line defect has not been well addressed earlier.

To explore it, we present in Fig. 5 the energy band diagrams for some typical AGNRs in presence of a line defect, where the defect sites are described by the yellow circles as shown in Fig. 1. The location of a line defect is described by the variable  $N_i$  and we assign  $N_i = 1$  for the edge of an AGNR. In Figs. 5(a) and (b) the results are shown for the ribbon widths  $N_y = 3n$  and  $3n + 1$ , respectively, and both for these two cases a finite energy gap around  $k_x = 0$  is obtained which reveals the semicon-

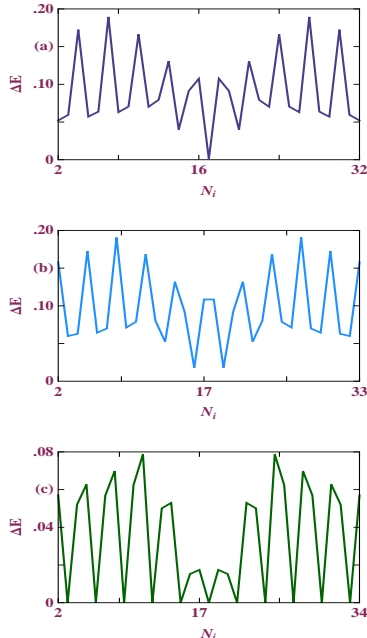


FIG. 6: (Color online). Energy gap  $\Delta E$ , at  $k_x = 0$ , as a function of impurity position  $N_i$  when (a)  $N_y = 33$ , (b)  $N_y = 34$ , and (c)  $N_y = 35$ .

ducting nature. The situation is somewhat interesting when the width of the AGNR gets the form  $3n + 2$ . The results are shown in Figs. 5(c) and (d) where we choose  $N_y = 20 (= 3 \times 6 + 2)$  and locate the defect lines at 6 and 5, respectively. In one case a sharp crossing between the energy levels takes place at  $k_x = 0$ , results a metallic phase, while for the other case a finite energy gap opens up for this typical value of  $k_x$  revealing the semiconducting phase. Thus, a metallic AGNR (width  $N_y = 3n + 2$ ) can exhibit a metallic or a semiconducting phase depending on the location of a impurity line in the ribbon. In a metallic AGNR two types of states, metallic and semiconducting, for carbon chains exist which result these two types of conducting phases depending on the location of line defect, while a semiconducting AGNR contains only semiconducting chains, and accordingly, it does not provide the metallic behavior in presence of a line defect.

The energy gap  $\Delta E$ , across  $k_x = 0$ , strongly depends

on the structural details i.e., the location of defect line in the nanoribbon. As illustrative example, in Fig. 6 we show the variation of  $\Delta E$  as a function of impurity position  $N_i$  for three different ribbon widths. It shows an oscillating behavior with the position of the defect line. For the semiconducting AGNRs (Figs. 6(a) and (b)) the energy gap never drops to zero, while for the metallic ribbon (Figs. 6(c))  $\Delta E$  vanishes when  $N_i$  becomes equal to  $3p$ ,  $p$  being an integer. These phenomena promote a design concept based on the structural details as semiconducting devices with variable energy band gaps.

## B. AGNR with side-attached leads: Two-terminal transmission probability and ADOS

Keeping in mind a possible experimental realization of the system, we clamp a finite sized armchair graphene nanoribbon between two ideal semi-infinite graphene leads (the left and right leads) making a lead-AGNR-lead bridge (see Fig. 1). Below we present our numerical

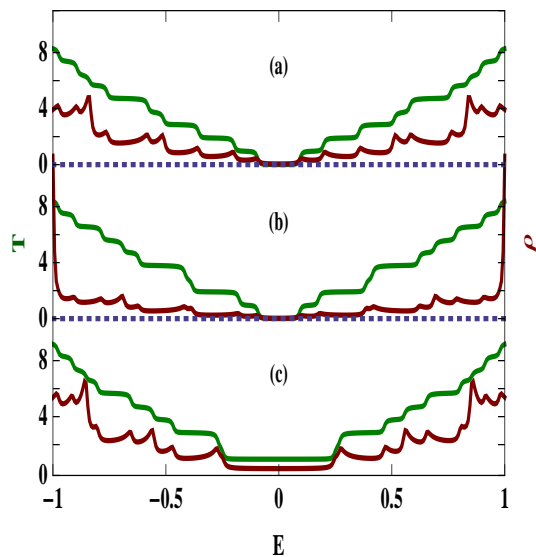


FIG. 7: (Color online). Transmission probability (green color) and average density of states (red color) for some typical armchair graphene nanoribbons in absence of line defect, where (a), (b) and (c) correspond to  $N_y = 3n$ ,  $3n + 1$ , and  $3n + 2$ , respectively. Here we set  $n = 6$  and take twenty unit cells.

results for average density of states (ADOS) and two-terminal transmission probability through finite sized AGNRs under conventional biased conditions.

In Fig. 7 we show the variation of transmission probability,  $T$ , together with the average density of states (ADOS),  $\rho$ , as a function of energy  $E$  for some typical finite sized AGNRs in the absence of any line defect, where (a), (b) and (c) correspond to the results for  $N_y = 3n$ ,  $3n + 1$  and  $3n + 2$ , respectively. Here we set  $n = 6$  and

choose twenty unit cells. Our previous analytical arguments for the AGNRs are exactly corroborated in these diagrams. A finite energy gap in the transmission probability associated with the energy gap in ADOS spectrum is obtained when  $N_y$  becomes identical to  $3n$  and  $3n + 1$ , as shown in Figs. 7(a) and (b). This behavior emphasizes the semiconducting phase for these ribbon widths.

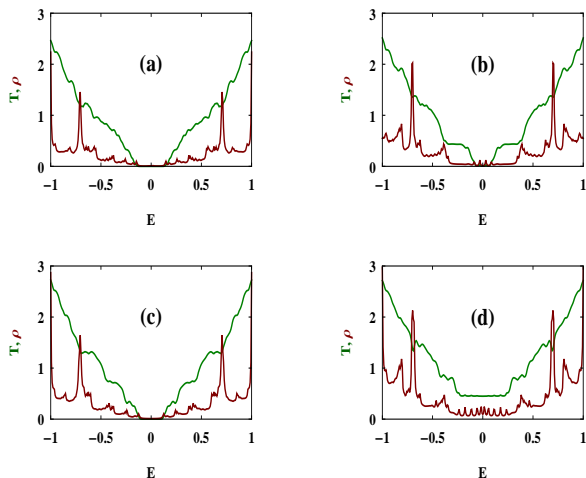


FIG. 8: (Color online). Transmission probability (green color) and average density of states (red color) for some typical armchair graphene nanoribbons in presence of single line defect. In (a) and (b) the results are shown for  $N_y = 3n$  and  $3n + 1$ , respectively, considering  $N_i = 5$ , while in (c) and (d) the results are given for  $N_y = 3n + 2$  when the defect line is placed at 5-th ( $N_i = 5$ ) and 6-rd ( $N_i = 6$ ) lines, respectively. Here we take twenty unit cells and fix  $n$  at 6.

On the other hand a gap less spectrum is observed when  $N_y$  becomes equal to  $3n + 2$  (Fig. 7(c)), which indicates the metallic phase of the AGNR.

Finally, we describe the results shown in Fig. 8, where we present transmission probability and ADOS for some typical AGNRs in presence of single line defect. In (a)

and (b) the results are presented for  $N_y = 3n$  and  $3n + 1$ , respectively, and for both these two cases transmission function shows a finite energy gap across  $E = 0$  exhibiting the semiconducting nature, with reduced amplitude compared to the spectra given in Fig. 7. The structural dependence on the conducting behavior in metallic AGNR ( $N_y = 3n + 2$ ) in presence of line defect is clearly visible from the spectra given in Figs. 8(c) and (d), where the defect lines are placed in the 4-th and 3-th lines, respectively. For the first case, it provides the semiconducting behavior, while in the other case the metallic phase is obtained, which perfectly corroborate our previous analytical findings.

#### IV. CONCLUSION

To summarize, we have investigated in detail the characteristics of energy band spectrum of armchair graphene nanoribbons in presence of line defect within a simple non-interacting tight-binding framework. The essential results have been presented in two parts. In the first part we have presented analytical results of energy band spectrum for isolated AGNRs. From our analytical results we have analyzed that depending on the location of a line defect a metallic AGNR can provide either a metallic or a semiconducting phase, while a semiconducting AGNR provides only the semiconducting phase with variable band gap. In the second part, we have discussed numerical results for transmission probability together with ADOS, keeping in mind a possible experimental realization of the system. We have shown that our numerical results exactly corroborate the analytical findings. Though the results presented in this article are worked out at absolute zero temperature limit, the results should remain valid even at finite temperatures ( $\sim 300$  K) since the broadening of the energy levels of the AGNR due to its coupling with the metal leads is much higher than that of the thermal broadening<sup>25,33–36</sup>.

\* Electronic address: paramita.dutta@saha.ac.in

† Electronic address: santanu.maiti@isical.ac.in

‡ Electronic address: sachindranath.karmakar@saha.ac.in

<sup>1</sup> K. S. Novoselov, A. K. Geim, S. V. Morozov, D. Jiang, Y. Zhang, S. V. Dubonos, I. V. Grigorieva, and A. A. Firsov, *Science* **306**, 666 (2004).

<sup>2</sup> A. H. C. Neto, F. Guinea, N. M. R. Peres, K. S. Novoselov, and A. K. Geim, *Rev. Mod. Phys.* **81**, 109 (2009).

<sup>3</sup> D. S. L. Abergel, V. Apalkov, J. Berashevich, K. Ziegler, and T. Chakraborty, *Adv. Phys.* **59**, 261 (2010).

<sup>4</sup> P. Dutta, S. K. Maiti, and S. N. Karmakar, *Eur. Phys. J. B* **85**, 126 (2012).

<sup>5</sup> V. Barone, O. Hod, and G. E. Scuseria, *Nano Lett.* **6**, 2748, (2007).

<sup>6</sup> K. Nakada, M. Fujita, G. Dresslhaus, and M. S. Dresslhaus, *Phys. Rev. B* **54**, 17954 (1996).

<sup>7</sup> Y. Ouyang, S. Sanvito, and J. Guo, *Surf. Sci.* **605**, 1643 (2011).

<sup>8</sup> B. Huang, *Phys. Lett. A* **375**, 845 (2011).

<sup>9</sup> S. H. R. Sena, J. M. Pereira Jr., G. A. Farias, F. M. Peeters, and R. N. Costa Filho, *J. Phys.: Condens. Matter* **24**, 375301 (2012).

<sup>10</sup> C. P. Chang, B. R. Wu, R. B. Chen, and M. F. Lin, *J. Appl. Phys.* **101**, 063506 (2007).

<sup>11</sup> Z. F. Wang, Q. Li, H. Zheng, H. Ren, H. Su, Q. W. Shi, and J. Chen, *Phys. Rev. B* **75**, 113406 (2007).

<sup>12</sup> H. Tsuyuki, S. Sakamoto, and M. Tomiya, arXiv:1207.5598.

<sup>13</sup> J. Lahiri, Y. Lin, P. Bozkurt, I. I. Oleynik, and M. Batzill, *Nature Nanotech.* **5**, 326 (2010).

<sup>14</sup> X. Lin and J. Ni, *Phys. Rev. B* **84**, 075461 (2011).

<sup>15</sup> S. Okada, T. Kawai, and K. Nakada, *J. Phys. Soc. Japan*

- 80**, 013709 (2011).
- <sup>16</sup> D. Gunlycke and C. T. White, Phys. Rev. Lett. **106**, 136806 (2011).
  - <sup>17</sup> R. N. Costa Filho, G. A. Farias, and F. M. Peeters, Phys. Rev. B **76**, 193409 (2007).
  - <sup>18</sup> M. Fujita, K. Wakabayashi, K. Nakada, and K. Kusakabe, J. Phys. Soc. Japan **65** 1920 (1996).
  - <sup>19</sup> K. Wakabayashi, Y. Takane, M. Yamamoto, and M. Sigrist, Carbon **47**, 124 (2009).
  - <sup>20</sup> M. Y. Han, B. Ozyilmaz, Y. B. Zhang, S. Lee, and H. Dai, Science **319**, 1229 (2008).
  - <sup>21</sup> D. R. Cooper, B. D'Anjou, N. Ghattamaneni, B. Harack, M. Hilke, A. Horth, N. Majlis, M. Massicotte, L. Vandsburger, E. Whiteway, and V. Yu, arXiv:1110.6557v1.
  - <sup>22</sup> H. Zheng, Z. F. Wang, T. Luo, Q. W. Shi, and J. Chen, Phys. Rev. B **75**, 165414 (2007).
  - <sup>23</sup> Y. -W. Son, M. L. Cohen, and S. G. Louie, Phys. Rev. Lett. **97**, 216803 (2006).
  - <sup>24</sup> X. Chen, H. Wang, H. Wan, K. Song, and G. Zhou, J. Phys.: Condens. Matter **23**, 315304 (2011).
  - <sup>25</sup> S. Datta, *Electronic transport in mesoscopic systems*, Cambridge University Press, Cambridge (1995).
  - <sup>26</sup> M. P. López Sancho, J. M. López Sancho, and J. Rubio, J. Phys. F: Met. Phys. **14**, 1205 (1984).
  - <sup>27</sup> M. B. Nardelli, Phys. Rev. B **60**, 7828 (1999).
  - <sup>28</sup> V. Meunier and B. G. Sumpter, J. Chem. Phys. **123**, 24705 (2005).
  - <sup>29</sup> E. Jóder, A. Pérez-Garrido, A. D'Áz-Sánchez, Phys. Rev. B **73**, 205403 (2006).
  - <sup>30</sup> A. A. Farajian, R. V. Belosludov, H. Mizuseki, Y. Kawazoe, Thin Solid Films **499**, 269 (2006).
  - <sup>31</sup> T. C. Li and S. P. Lu, Phys. Rev. B **77**, 085408 (2008).
  - <sup>32</sup> F. Khoeini, A. A. Shokri, and F. Khoeini, Eur. Phys. J. B **75**, 505 (2010).
  - <sup>33</sup> P. Dutta, S. K. Maiti, and S. N. Karmakar, Solid State Commun. **150**, 1056 (2010).
  - <sup>34</sup> P. Dutta, S. K. Maiti, and S. N. Karmakar, Org. Electron. **11**, 1120 (2010).
  - <sup>35</sup> M. Dey, S. K. Maiti, and S. N. Karmakar, Org. Electron. **12**, 1017 (2011).
  - <sup>36</sup> S. K. Maiti, Phys. Scr. **75**, 62 (2007).